Infrared Spectrum of an Acidic Zeolite OH with Adsorbed Acetonitrile

E. L. Meijer,* R. A. van Santen, and A. P. J. Jansen

Eindhoven University of Technology, Schuit Institute of Catalysis, Theory Group, P.O. box 513, 5600 MB Eindhoven, The Netherlands

Received: August 4, 1998; In Final Form: February 9, 1999

The effect of acetonitrile adsorption on the infrared spectrum of an acidic hydroxyl group of a zeolite was studied using quantum-chemical calculations. The hydroxyl and its surroundings in the zeolite were modeled by a cluster molecule. Potential energy and dipole surfaces of the model were computed with density functional theory applying the Becke3LYP functional. A potential energy surface has been constructed as a function of the stretch, in-plane bending, and out-of-plane bending coordinates of both the hydrogen and the oxygen atom of the hydroxyl group, as well as the center-of-mass stretch coordinate of acetonitrile. Taking into full account anharmonicities, we computed the vibrational wave functions and infrared absorption intensities using a variational approach. To facilitate their interpretation, the computed spectra were decomposed with respect to the different vibrational coordinates. It was found that the use of center of mass conserving coordinates for the hydroxyl group is insufficient to obtain accurate hydroxyl stretch frequencies, and that oxygen coordinates need to be included in the calculation. The inclusion of oxygen coordinates furthermore improves the computed Fermi resonance splitting. A new explanation for the width of the A,B spectra is proposed.

Introduction

Zeolites are crystalline materials consisting mainly of SiO_4 tetrahedra that are linked through sharing of oxygen atoms. They appear in many different crystal structures that exhibit channels and cages of molecular dimensions 4−12 Å. In most zeolites a fraction of the silicon atoms is replaced by aluminum atoms. The negative charge this introduces into the lattice can be balanced by a proton attached to the oxygen atoms that bridges a silicon and an aluminum atom, thus forming a bridged hydroxyl with strong Brønsted acidity. The combination of these acidic sites with the well-defined micropores makes them suitable catalysts for a range of reactions.

In the infrared spectrum of a zeolite, the bridged hydroxyl stretch mode is observed in the range 3605−3615 cm^{-1}. If a weakly basic molecule is adsorbed on the hydroxyl, the stretch frequency shifts to lower values. The shift that occurs with a certain base molecule has been proposed as a measure for the acidity of the bridging hydroxyl (see ref 1 and references therein). For this application weak bases such as CO and N_2 that only cause small shifts are most suitable.[2,3]

Acetonitrile is among the strongest basic molecules that will disturb a bridging hydroxyl, but not subtract a proton from it. The infrared spectrum resulting is more complicated than that of weaker bases. It displays a large downward shift (800−1200 cm^{-1}) of the hydroxyl stretch band, as well as a marked splitting and broadening of the band. The resulting two main broad bands at 2400 and 2800 cm^{-1} are usually referred to as the A,B-diad. Sometimes a third band, denoted "C" is seen at even lower frequencies. This band is usually less clear. Conclusive experimental evidence exists that these bands are due to one single type of complex, where acetonitrile is hydrogen bonded to the bridging hydroxyl.[1,4,5]

The characteristic splitting of the shifted hydroxyl stretch band into the A,B-diad is caused by a Fermi resonance between a broadened hydroxyl stretch band (ν) and the overtone of the in-plane (δ) hydroxyl bending, where the "plane" refers to the plane formed by the Si−O−Al group on which the extra proton sits.

Empirical models have been applied to describe the spectra.[6−8] In earlier work we tried to compute the infrared spectrum from first principles,[9] taking into account only a minimal set of vibrational coordinates: the coordinates of the hydrogen atom of the hydroxyl group and the intermolecular stretch of the acetonitrile molecule as a whole with respect to the hydroxyl. Using this simple model we could show that among the vibrational wave functions computed on the basis of a density functional potential energy surface Fermi resonances did occur. However, the computed width of the A,B bands, the size of the A,B splitting, and the stretch frequency of the free bridged hydroxyl left room for improvement. In the current paper we present the results of an extension of the former model to include the dynamics of the oxygen atom. Based on this model, we propose an interpretation of the nature of the A,B-spectra that differs from the empirical models mentioned.

Computational Details

Potential Energy and the Dipole Surfaces. The acidic OH group of the zeolite is represented by a small, neutral, cluster molecule, terminated by hydroxyl groups. This model is shown in Figure 1, along with the coordinates we used in the vibrational calculations. All coordinates are linear combinations of atomic displacements. Electronic structure calculations have been used to compute potential energy and dipole surfaces as a function of a limited number of degrees of freedom.

In a previous paper,[9] where we presented calculations of anharmonic coupling effects, we only considered the stretch, in-plane, and out-of-plane coordinates of the hydrogen atom, and the stretch of the H···N hydrogen bridge, with acetonitrile as a rigid particle. Here we also include the movement of the oxygen atom of the OH group for the acidic OH group and the acidic OH group with adsorbed acetonitrile. We extended the

10.1021/jp983263c CCC: $18.00
Published on Web 03/27/1999

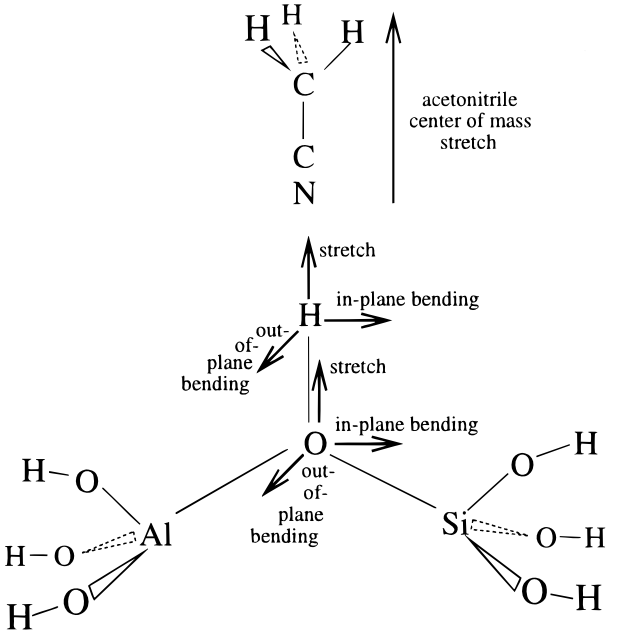

Figure 1. Zeolite cluster model with adsorbed acetonitrile. The vibrational coordinates used in the calculations are shown as arrows.

potential energy and dipole surfaces used in the previous work to obtain 6- and 7-dimensional versions.

The potential energy surfaces used are based on density functional theory electronic structure calculations using Becke's three-parameter functional with the nonlocal correlation provided by the Lee, Yang, and Parr expression.[10−13] We have demonstrated earlier[9] that this method gives results that are significantly better than those obtained with Hartree−Fock. Therefore we have not extended the Hartree−Fock potentials from the previous work. The electronic structure calculations have been carried out with the Gaussian 92/DFT program package.[14] A mixed basis set has been used with STO-3G[15] on the H atoms of the terminal OH groups, 6-311+G* [16−18] on the central O atom of the zeolite cluster and the N atom of acetonitrile, and 6-31G** [19−22] for the other atoms. This basis set describes the atoms that are important in the interaction between the acidic hydroxyl and the acetonitrile molecule accurately.[9] The minimal basis set on the terminal hydrogen atoms of the cluster was used to reduce computational costs.

As a starting point for the potential energy surfaces, the zeolite cluster as shown in Figure 1 was optimized with and without adsorbed acetonitrile. The optimization was restricted in two ways. First, during the optimization, the plane through the central Si−OH−Al group was kept as a mirror plane, to reduce the number of points that had to be computed for the potential energy surface. Second, to prevent internal hydrogen bridging, the Si−O−H and Al−O−H angles of the terminating OH groups were fixed at tetrahedral angles, and going from the central O atom to a terminal OH, O−Si−O−H and O−Al−O−H atoms were required to stay in one plane.

The three-dimensional potential energy surface is the potential energy of the zeolite cluster as a function of the acidic hydrogen coordinates. It is based on electronic structure calculations performed for a grid of acidic hydrogen positions. The grid was constructed as follows: At five different OH distances, 0.8, 0.9, 1.0, 1.1, and 1.4 times the equilibrium distance, the hydrogen atom was bent toward the Al atom by an angle θ of 0°, 7.5°, 20°, and 60° and subsequently rotated around the axis defined by the equilibrium acidic OH bond by an angle ϕ of 0°, 45°, 90°, 135°, and 180°. The energies and dipoles of geometries corresponding to $\phi = 225°$, 270°, and 315° were inferred from the 135°, 90°, and 45° points by taking into account the symmetry plane of the cluster.

The four-dimensional potential describes the energy of the zeolite cluster with a molecule of acetonitrile adsorbed as a function of the acidic hydrogen coordinates and the acetonitrile center of mass stretch coordinate. All internal acetonitrile coordinates were kept fixed. A grid of hydrogen positions has been constructed in the same fashion as for the bare zeolite cluster, using the equilibrium OH distance in the acidic hydroxyl with acetonitrile adsorbed. For each of the points of this grid the electronic energy was computed for five different distances between acetonitrile and the oxygen atom of the zeolite acidic OH group: the equilibrium distance r_0, $r_0 \pm 0.15$ Å, and $r_0 \pm 0.5$ Å. The potential energy points were fitted with fourth-order polynomials. For the fit each point i was attributed a fit weight w_i according to the following expression:

$$w_i \equiv \frac{e^{-fv_i}}{\sum_j^N e^{-fv_j}} \qquad (1)$$

Here v_i is the electronic energy of point i, N is the total number of points, and f is a positive factor that determines the relative weight of the points. This expression attributes larger fit weights to data points with lower potential energies. Physically, data points with low energy are relatively more significant for the correct description of the lower lying vibrational levels, which we want to describe. The f parameter was given a value of $125E_h^{-1}$, so as to produce a root-mean-square error smaller than $1 \times 10^{-3}E_h$. The computed energies for potentials were in an interval of approximately $0.2E_h$.

All fits in this paper were performed with singular value decomposition,[23] in order to remove near-degeneracies. For the three and four-dimensional fits we had to set one of the singular values to zero. This means that one degree of freedom of the polynomial was fixed through minimization of the squares of the coefficients.

Both the three and four-dimensional potential had negative fourth order coefficients for the hydrogen stretch coordinate. If basis functions were allowed to extend into the area where the fitted potential approached negative infinity, unphysical vibrational wave functions would be computed. We have shown earlier[9] that this problem does not occur in our three- and four-dimensional calculations, since the wave functions stay confined to an area where the fitted potential interpolates between the computed data points.

The six-dimensional potential describes the potential energy of the zeolite cluster, as a function of the position of the oxygen and hydrogen atoms of the acidic OH group. In its construction, the coefficients of the three-dimensional potential for hydrogen displacement have been retained. The second-order coefficients for the oxygen coordinates and the bilinear coupling coefficients for the oxygen coordinates among themselves, and with the hydrogen coordinates, have been derived from the force constants computed in a Gaussian92 normal mode calculation. The potential thus constructed did not display the desired asymptotic behavior for large displacements of the atoms from their origins. In certain directions, already at relatively small distances from the equilibrium, the potential showed large negative values, giving rise to the computation of unphysical vibrational states.

To improve the potential, extra data points of the potential energy surface have been computed. The grid of extra points

can be described in terms of displacement vectors of oxygen and hydrogen. We define $\mathbf{x}_1$ to be a vector along the OH bond, $\mathbf{x}_2$ a vector in the direction perpendicular to the OH bond in the Al−O−Si plane, and $\mathbf{x}_3$ a vector perpendicular to $\mathbf{x}_1$ and $\mathbf{x}_2$.

Initially, a grid has been constructed from molecular geometries where oxygen or both oxygen and hydrogen were displaced by $\pm\mathbf{x}_1$, $\pm\mathbf{x}_2$, $\pm\mathbf{x}_3$, or $\pm(\mathbf{x}_1 + \mathbf{x}_2 + \mathbf{x}_3)/\sqrt{3}$. The lengths of the vectors $\mathbf{x}_i$ are derived from the force constants in the corresponding directions, in such a way that the displacements correspond to 8 times the root-mean-square (rms) displacement of a one-dimensional harmonic vibration of the atom. This means that the vectors for hydrogen displacement have different lengths from those for oxygen. The fitted second-order coefficient of the potential energy with respect to the out-of-plane movement of hydrogen is negative. This displacement has its length derived from the force constant used for the basis function, as described in ref 9.

In some of the geometries generated in this grid the OH distance becomes as small as 0.16 Å. Therefore we have applied a correction to the grid points through expansion of the OH bond about its center of mass. The new OH distance was computed from the old via a linear transformation that leaves the maximum distance from the grid as it is and expands the smallest distance to 0.5 times the equilibrium distance of the OH bond. If the maximum distance in the original grid is r_{max}, the minimum distance r_{min}, and the equilibrium OH distance r_{eq}, then the new OH distances r' are computed from the old r using

$$r' = r + \frac{(r_{max} - r)}{(r_{max} - r_{min})}(r_{eq}/2 - r_{min}) \qquad (2)$$

The grid contains 210 points, which were attributed fit weights, as described in eq 1, again with $f = 125E_h^{-1}$. In the singular value decomposition procedure we had to set 47 singular values to zero. This means that 47 degrees of freedom in the polynomial were left that were fixed by minimizing the sum of the squares of the fitted coefficients. The potential so obtained proved suitable for our calculations and no unphysical vibrational states were found with the basis set we employed.

The seven-dimensional potential energy surface describes the potential energy of the zeolite cluster with adsorbed acetonitrile as a function of the coordinates of the acidic OH group of the cluster and the center of mass stretch of acetonitrile. It has been constructed by retaining the coefficients of the four-dimensional potential, and quadratic terms for the oxygen movement and bilinear coupling terms between oxygen and hydrogen coordinates have been derived from a Gaussian normal mode calculation. Coupling terms between the oxygen coordinates and the acetonitrile coordinate have been neglected, because although they are small and have little physical importance, they can give rise to problems with the asymptotic behavior of the fitted polynomial if no higher order coefficients are included as well.

As in the case of the six-dimensional potential, extra points of the potential energy surface had to be computed, and a grid similar to the one described for the six-dimensional surface was employed. No extra points were used to further probe the coupling of the oxygen coordinates and the acetonitrile coordinate. The grid of the extra points for the seven-dimensional potential was constructed with vectors $\mathbf{x}_i$ (see above) of a length 4 times the one-dimensional harmonic rms displacement of the atom. This is much nearer to the origin than in the six-dimensional case, where the larger displacements were necessary to get satisfactory asymptotic behavior of the fitted potential. Because of the smaller displacements there was no need to adjust the grid points afterward to prevent too small interatomic distances.

Fit weights were attributed to the extra points in the same manner as in the six-dimensional case. In this case 41 singular values had to be set to zero.

For all the data points we used for the three- and the four-dimensional potential energy surfaces, also the *x*, *y*, and *z* components of the dipole were computed. Using the same fit weights as for the energy, the dipole surfaces were fitted by fourth-order polynomials.

To reduce computational cost we only used linear dipole surfaces for both the six- and the seven-dimensional spectra. For the hydrogen and acetonitrile coordinates the dipole coefficients up to first order computed from the three- and four-dimensional surfaces were used, for the oxygen coordinates the dipole and dipole derivatives computed in a Gaussian92 normal mode calculation were used.

From the three- and four-dimensional calculations it appears that the computed spectra are hardly affected by the omission of higher order dipole coefficients. As a test case we computed for the four-dimensional spectrum that the total absorbed intensity of the infrared spectrum at 298.15 K, in the range of 0−4000 cm^{-1}, decreases by 0.35%, comparing a linear dipole surface to a fourth-order dipole surface. For that same spectrum, the root-mean-square difference in intensity on a per transition basis was about 3.2%. Clearly, differences exist in both positive and negative directions and are of minor importance.

Calculation of the Infrared Spectra

Vibrational Hamiltonian. The Hamiltonian employed in the vibrational calculations is the following:

$$H = \frac{1}{2}\sum_{i=1}^{D}\sum_{j=1}^{D} M_{ij}^{-1} p_i p_j + \sum_{\alpha_1,\ldots,\alpha_D} a_{\alpha_1,\ldots,\alpha_D} \prod_{i=1}^{D} q_i^{\alpha_i} \qquad \text{with}$$

$$0 \le \sum_{i=1}^{D} \alpha_i \le N \qquad (3)$$

In this expression D is the number of dimensions, q_i are the spatial coordinates with conjugated momenta p_i, $\boldsymbol{M}^{-1}$ is the inverse mass matrix, and $a_{\alpha_1,\ldots,\alpha_D}$ are the coefficients of the Nth order polynomial representing the potential energy.[24] For all the calculations in this paper, the polynomial order N has been equal to 4. The way the potential energy polynomial is truncated ensures that its shape does not depend on a particular choice of internal coordinates. (It should be noted, however, that the wave function space spanned by the basis set is not independent from the choice of the coordinates.)

We choose to use a polynomial representation of the potential because it has no bias toward a particular potential shape, and matrix elements can be readily computed in the basis set we employed. To this effect, the Hamiltonian was converted into a representation of normal products of creation and annihilation operators.[25]

A disadvantage of the polynomial form of the potential is the unphysical behavior of the potential outside the area where data points were computed. A polynomial potential goes to $\pm\infty$, where a physical potential levels off to a constant value. This is mainly a concern if the polynomial goes to $-\infty$. As a result, unphysical low-energy vibrational states can occur in the calculation, if the basis functions have a nonnegligible amplitude

in the area where the potential has unphysically low values. We have avoided such basis functions.

The off-diagonal terms $M_{ij}p_i\,p_j$ in the kinetic energy can have nonzero values if the coordinates are not orthogonal. This was never the case in the calculations described in this paper.

The wave functions are expanded in products of one-dimensional harmonic eigenfunctions (Hermite functions).[24]

$$\psi(q_1,...,q_D) = \sum_{\alpha_1,...,\alpha_D} c_{\alpha_1,...,\alpha_D} \prod_{i=1}^{D} \phi^{(\alpha_i)}(q_i) \tag{4}$$

In this expression ψ is the vibrational wave function in D dimensions and $\phi^{(\alpha_i)}(q_i)$ is the normalized α_ith-order Hermite function of coordinate q_i. The basis was truncated by specifying a maximum value N_i for each α_i and subsequently imposing the following condition for each basis function:

$$\sum_{i=1}^{D} \frac{\alpha_i}{N_i} \le 1 \tag{5}$$

In the case of a harmonic potential this limits the total energy of any basis function to the highest energy one-coordinate basis function plus the zero-point energy of the other one-coordinate basis functions.

In the computations in the current work we used $N_i = 12$ for the hydrogen and acetonitrile coordinates, and $N_i = 6$ for the oxygen coordinates. The main reason not to extend the basis set on the oxygen coordinates to 12 as well was to keep the calculations feasible. On a physical basis it can be argued that a larger basis on the hydrogen coordinates is needed: the hydrogen atom is more subject to anharmonicities in the potential due to its smaller weight and hence larger amplitude. The basis sets contained 455, 1820, 3906, and 11 286 functions for the three-, four-, six-, and seven-dimensional models, respectively.

The one-dimensional Hermite functions are characterized by the quotient of a force constant and a mass. For the mass we used $1/(M_{ii}^{-1})$ as defined in eq 3. The force constant was derived from the second-order coefficient of the coordinate in the potential energy. For the out-of-plane bending coordinate of hydrogen in the zeolite cluster without acetonitrile, this coefficient was negative, and the force constant was derived from the rms deviation of the anharmonic wave function in this coordinate. This procedure was described in more detail in ref 9.

We computed integrated infrared absorption intensities applying Fermi's golden rule[26] and fractional Boltzmann occupation numbers at a given temperature. The integrated absorption intensity $A_{i\to f}$ from initial level i to final level f is given by

$$A_{i\to f} = \frac{2\pi^2 \Delta E}{3\epsilon_0 h^2 c^2} \sum_{\alpha=x,y,z} |\langle i|\mu_\alpha|f\rangle|^2 \frac{e^{-E_i/kT}}{\sum_j^N e^{-E_j/kT}} \tag{6}$$

In this expression $A_{i\to f}$ is defined for one particle per unit surface, integrated over wavenumbers and averaged over different molecular orientations. ΔE is the difference in energy between the normalized states $|i\rangle$ and $|f\rangle$, ϵ_0 is the electrical permittivity of vacuum, h is Planck's constant, c is the speed of light in a vacuum, μ_x, μ_y, and μ_z are the components of the dipole operator, E_j is the energy of vibrational level j, k is the Boltzmann constant, T is the absolute temperature, and N is the number of vibrational states taken into account.

In the computation of the matrix elements $\langle i|\mu_\alpha|f\rangle$ from eq 6 the electric anharmonicities, i.e., second-order and higher terms in the dipole components, were taken into account for the three- and four-dimensional models. As discussed earlier, we only used linear terms of the dipole components in the six- and seven-dimensional models. Mechanical anharmonicities, i.e., third-order and higher terms in the potential energy, were incorporated in all calculations. To facilitate the computation of transition dipoles, the dipole components were converted into a representation of normal products of creation and annihilation operators.

Modified Lanczos Algorithm

The computations on the six- and seven-dimensional systems are much larger than those on the three- and four-dimensional ones in the previous work in two respects: the basis sets are larger, and the numbers of levels that need to be computed to find the first excited state of the OH stretch mode are larger. Because the fundamental frequencies of the oxygen modes are very low compared to the hydrogen stretch mode, the number of extra modes that need to be computed for the six- and seven-dimensional spectra are even larger than should be expected from the added dimensions alone. The computation of the eigenvectors, which we use to obtain absorption intensities and to analyze the levels, entails large computer memory usage and CPU time consumption in the simple Lanczos algorithm we used for the three- and four-dimensional models. Furthermore, it appeared that at a certain, insufficient, number of computed energy levels, we could not obtain extra levels by increasing the number of Lanczos iterations. To overcome these problems, we implemented a slightly modified Lanczos scheme, as described by Lewis in his Ph.D. thesis.[27]

In a Lanczos procedure, extreme eigenvalues, and eigenvalues that are well separated, can be obtained with a small number of iterations. The method we employed improves the separation of the eigenvalues in the interval we are interested in, relative to the separation of eigenvalues outside that interval. We start by computing the extreme eigenvalues $E_{\min}$ and $E_{\max}$ of the Hamiltonian H, which is easily done with an ordinary Lanczos scheme. Then we determine the interval $[E_{\min},E_0]$ in which we want to find the eigenvalues and construct a polynomial f such that it maps $[E_{\min},E_0]$ to $[f_{\min},f_0]$ and $[E_0,E_{\max}]$ to $[f_0,f_{\max}]$. Furthermore, f is monotonic on $[E_{\min},E_0]$, and constructed such that

$$Q_{\text{stretch}} \equiv \frac{(f_0 - f_{\min})/(f_{\max} - f_0)}{(E_0 - E_{\min})/(E_{\max} - E_0)} \gg 1 \tag{7}$$

Figure 2 shows such a polynomial of fourth order, which has a Q_{stretch} of 34.5. This means that the relative part of the eigenspectrum occupied by the eigenvalues we are interested in is larger by a factor of 34.5 in comparison of the transformed Hamiltonian to the original one. The Hamiltonian H and the operator $f(H)$ share the same set of eigenvectors, but the eigenvalues of $f(H)$ corresponding to those of H in $[E_{\min},E_0]$ are better separated. We diagonalize $f(H)$ by employing an ordinary Lanczos procedure and use the computed eigenvectors $|\Psi_i\rangle$ to obtain the eigenvalues of H as $E_i = \langle\psi_i|H|\psi_i\rangle$.

For the six-dimensional calculation, a fourth-order polynomial was sufficient to compute 300 energy levels in 3000 Lanczos iterations, the highest level differing from the lowest by 3933

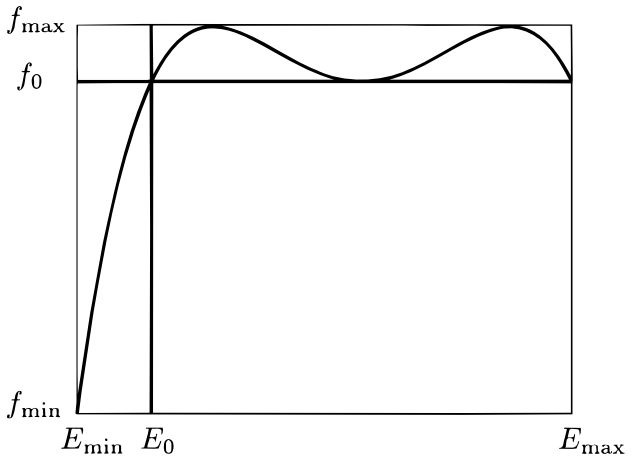

Figure 2. Polynomial to modify the eigenvalue spectrum of a Hamiltonian in order to improve separation of certain levels. On the horizontal axis are the eigenvalues of the original Hamiltonian, on the vertical axis, the corresponding eigenvalues of the new Hamiltonian.

cm^{-1}. The polynomial was constructed with $E_0 - E_{min} = 4000$ cm^{-1} and had a stretching quotient $Q_{stretch} = 19.2$.

To compute enough levels of the seven-dimensional system, we had to construct a ninth-order polynomial, starting with $E_0 - E_{min} = 5000$ cm^{-1}. This polynomial had a stretch quotient $Q_{stretch} = 188$, enabling us to compute 629 different energy levels in 4000 Lanczos iterations, with a difference of 4105 cm^{-1} between the highest and the ground level.

Note that the general trend is that both raising the order of the polynomial and shifting up the value of E_0 result in higher values of $Q_{stretch}$. One disadvantage of raising the order of the polynomial is that it increases CPU time consumption per Lanczos iteration. Another disadvantage is that it may cause deterioration of accuracy. The accuracy can, however, be easily monitored by calculating $\langle\psi_i|H|\psi_i\rangle \pm \sqrt{\langle\psi_i|H^2|\psi_i\rangle - |\langle\psi_i|H|\psi_i\rangle|^2}$,[28] which provides sharp boundaries in which an exact eigenvalue exists. This shows for our seven-dimensional calculations that four significant digits are present for all levels, whereas most levels are defined much sharper. Raising the value of E_0 too much eventually deteriorates the possibility of find eigenvalues in the desired area, because the number of well-separated eigenvalues that can be found increases.

Attribution of Peaks in the Infrared Spectrum

For the three- and four-dimensional models we used it was possible to identify different wave functions looking at the coefficients of the basis functions.[9] In the six- and seven-dimensional calculations it has become much more difficult to do so, because the used coordinates are strongly coupled. Typically, a wave function has a number of contributing basis functions with normalized coefficients having an absolute value of approximately 0.2, and often no obvious main component is present. We use the following method to determine whether a coordinate is involved in a certain transition in the infrared spectrum, and subsequently to compute partial spectra for each coordinate.

Suppose that the initial state ψ_i is given by

$$\psi_i = \sum_{\alpha_1,\ldots,\alpha_D} c_{\alpha_1,\ldots,\alpha_D} \prod_{j=1}^{D} \phi^{(\alpha_j)}(q_j) \qquad (8)$$

We form new states

$$\psi_i^{(k;\mathbf{n})} = \sum_{\alpha_1,\ldots,\alpha_D} c_{\alpha_1,\ldots,\alpha_D} \prod_{j=1}^{D} \phi^{(\alpha_j+n_j)}(q_j) \qquad (9)$$

with $n_k \neq 0$ and n_j with $j \neq k$ arbitrary. This corresponds to an excitation ($n_k > 0$) or de-excitation ($n_k < 0$) of the initial state in coordinate k, and possibly (de)-excitations in other coordinates as well. To determine if a transition from ψ_i to a final state ψ_f involves excitation in coordinate k, we projected ψ_f onto the space spanned by the $\psi_i^{(k;\mathbf{n})}$'s with $n_k > 0$. The contribution of the transition $\psi_i \rightarrow \psi_f$ in the partial spectrum of the excitation in coordinate k is the peak intensity of that transition times the norm of the projection. Taking $n_k < 0$, we can generate partial spectra for de-excitations.

Interpreting the partial spectra obtained in this way, one should keep in mind that they do not represent anything else but a computational version of comparing coefficients of basis functions. They have no measurable physical meaning, and are a function of the coordinates chosen. In the limit of a harmonic potential with the corresponding normal coordinates and a linear dipole surface the partial spectra add up to give the total infrared spectrum, and each partial excitation spectrum contains exactly the single transition belonging to its normal coordinate whereas the de-excitation spectra contain no peaks at all. In most other cases, the partial spectra add up to yield more than the total intensity of the total infrared spectrum. This happens because of the coupling of the coordinates. A transition in which two modes are simultaneously excited shows up with full intensity in both partial spectra. Partial spectra that would be additive can only be constructed with arbitrary partition schemes, very similar to the ones used in Mulliken population analysis.

Results and Discussion

Our calculations yield infrared transition frequencies and integrated absorption intensities, but no line widths. To generate the spectra shown in this paper, we convoluted Dirac delta functions with normalized Gaussian curves of width 10 cm^{-1}, multiplied by the absorption intensity. In the figures of the decomposed spectra, the intensity of the partial excitation spectra is plotted in the positive direction (up), and the de-excitation spectra are plotted in the negative direction (down). De-excitation spectra mostly contain peaks for the lower energy modes, because they involve thermally excited initial states. All spectra plotted in this paper are computed at a temperature of 298.15 K.

Figure 3 shows the computed infrared spectra for the three-dimensional (hydrogen coordinates only) and six-dimensional (oxygen and hydrogen coordinates) models. In the six-dimensional spectrum the area between the out-of-plane bending (ca. 400 cm^{-1}) and the in-plane bending mode (ca. 1100 cm^{-1}) contains many small combination peaks that contain contributions from the oxygen modes and the hydrogen bending modes. The oxygen modes in our model represent part of the dynamics of the Si−O and Al−O bonds, which cause the lattice modes in zeolites. The six-dimensional spectrum already shows that the lattice modes will interact with the out-of-plane hydroxyl bending mode.

The fundamental hydroxyl stretch frequency is found in the six-dimensional calculation at approximately 3522 cm^{-1}. The peak at 3575 cm^{-1} is a hot band where the hydroxyl stretch is excited from an initial state that is excited in the out-of-plane bending of oxygen. This peak is similar to the peak at 3558 cm^{-1} in the three-dimensional spectrum, which represents an excitation of the hydrogen stretch from an initial state in which the hydrogen out-of-plane bending is already excited (see also[9]).

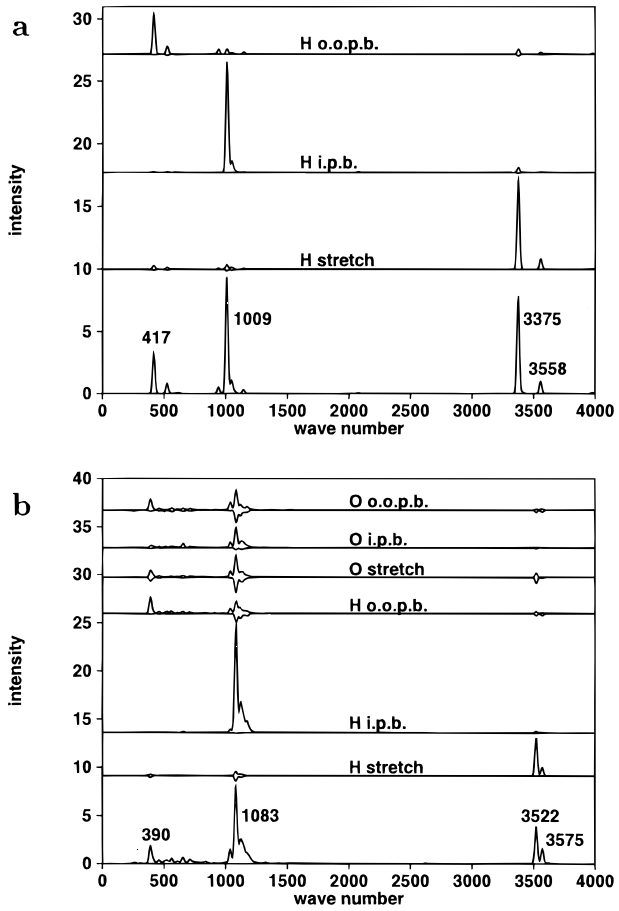

Figure 3. Decomposed infrared spectra of the zeolite hydroxyl group according to the three- (a) and six-dimensional (b) model. Wavenumbers are in cm^{-1}, intensity is in 10^5 m^2/mol. The spectrum on the bottom line represents the full infrared spectrum. From bottom to top then follow the partial spectra of the hydrogen stretch, in-plane bending, and out-of-plane bending and, for the six-dimensional model the partial spectra of the oxygen stretch, in-plane bending, and out-of-plane bending mode.

The hydroxyl stretch frequency of 3522 cm^{-1} computed in the six-dimensional spectrum is nearer to the experimental value around 3610 cm^{-1} than the value in the three-dimensional spectrum of 3375 cm^{-1}. In the six-dimensional model the reduced mass for the hydroxyl stretch mode is ca. 6% smaller than that of the corresponding hydrogen stretch in the three-dimensional model. If this were the main difference, it would in the harmonic case lead to an increase of the frequency by ca. 3%, or approximately 100 cm^{-1}. This amount is not enough to explain the observed difference.

To investigate the influence of the reduced mass further, we took three internal OH coordinates and computed an infrared spectrum using the corresponding three-dimensional intersection of the six-dimensional potential. For the hydrogen atom these coordinates were identical to those used for the older three-dimensional calculations, but also oxygen was moving so as to conserve the center of mass of the OH group. We found that the OH stretch frequency computed did not differ from the one in the old three-dimensional calculation. The explanation lies in the cancelation of two effects: on one hand the lower reduced mass would lead to a higher OH stretch frequency, whereas on the other hand the intersection of the potential energy well is flatter for the energy surface with the internal OH coordinates. The latter effect can physically be understood in terms of bond strengths. When the OH bond becomes longer, and oxygen is allowed to move in the opposite direction of hydrogen, the OAl and OSi bonds become shorter. This allows these bonds to become stronger at the same time the OH bond becomes weaker, causing a flatter potential energy well for the coordinate. When the OH bond shortens, the OAl and OSi bonds become longer, causing a small increase in energy. We found this effect to be smaller than the lowering of the energy for the longer OH bond. Moreover, for the vibrational frequency, the lower parts of the potential energy well are more important than the higher parts.

We find that a "reduced mass effect" in itself is not responsible for the difference in hydroxyl stretch frequency that is observed between our three- and six-dimensional models (Figure 3). An explanation for the fact that the six-dimensional spectrum does have a higher hydroxyl stretch frequency than the three-dimensional one should be found in the extra modes. The additional modes of the oxygen atom are low in energy and push the hydroxyl stretch mode up. It is therefore essential to include the oxygen modes as extra modes when computing stretch frequencies of bonded hydroxyl groups. The intuitively appealing one-dimensional approximation using a coordinate that retains the center of mass of the hydroxyl group, along with the reduced hydroxyl mass, can yield a stretch frequency that is too low.

The decomposed spectra in Figure 3 show that in the three-dimensional model the chosen coordinates represent modes that are almost normal to each other. In the six-dimensional calculation we see that all the modes included take part in the in-plane bending around 1100 cm^{-1}. The interaction between the modes clearly demonstrates that the set of coordinates used does not correspond to a set of normal modes.

In Figure 4 the decomposed spectra for the four- and the seven-dimensional models are plotted. Note that some of the peak positions written in Figure 4a differ from those reported in ref 9. The wavenumbers in our previous article corresponded to one transition, whereas in this article we used the maxima in the total spectrum as plotted in the figures. Because, especially in the higher dimensional spectra almost every peak is due to more than one transition, the positions of the maxima in the spectrum usually differ somewhat from the frequency of their principle component. In the case of the seven-dimensional spectrum there is sometimes no clear principle component.

The decomposed spectrum of the four-dimensional calculation (Figure 4), clearly shows the interaction between the hydrogen stretch and the hydrogen in-plane bending overtone. The in-plane bending mode has peaks on both sides of the "Fermi dip" at ca. 2600 cm^{-1}, whereas the stretch is predominantly present on the high-frequency side. The acetonitrile stretch interacts almost exclusively with the hydrogen stretch mode, causing a broadening of approximately 300 cm^{-1}.

In the four-dimensional spectra the following important transitions are visible. At 112 cm^{-1} the fundamental acetonitrile center of mass stretch is found. The out-of-plane hydrogen bending and its overtone are visible at 778 and 1690 cm^{-1}, respectively. At 1153 cm^{-1} we find the in-plane hydrogen bending mode; its overtone is at 2387 cm^{-1}. All these transitions can be readily identified from the partial spectra plotted in Figure 4a. The in-plane bending overtone at 2387 cm^{-1} has some slight interaction with the hydrogen stretch and the main hydrogen stretch peak at 2626 cm^{-1} shows substantial interaction with the in-plane bending overtone. This follows from looking at the coefficients of the basis functions of the involved states and also from the partial spectra in Figure 4a. The interaction between the in-plane bending overtone and the hydrogen stretch is a Fermi resonance. This is an interaction between two vibrational states that approximately have the same energy, not

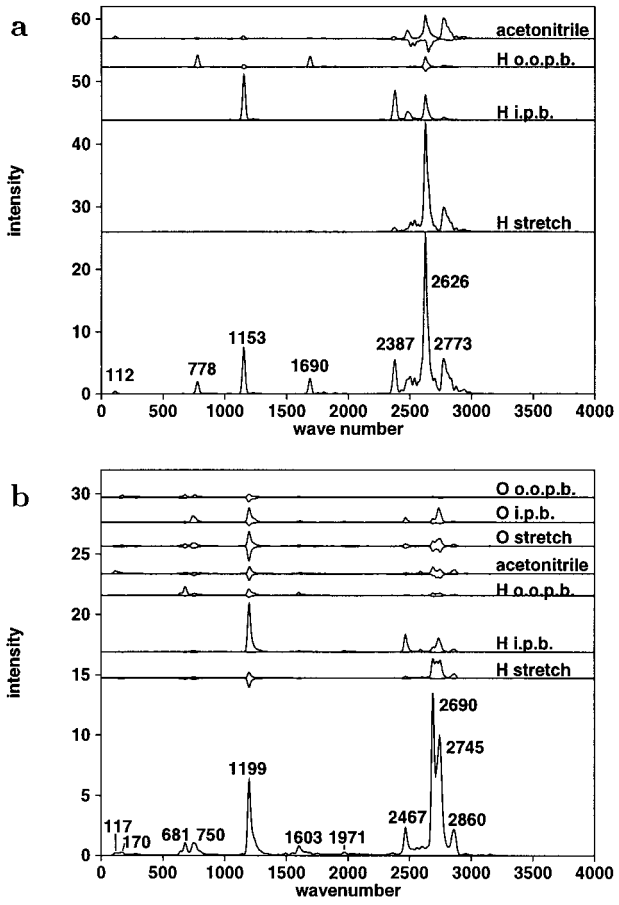

Figure 4. Decomposed infrared spectra of the zeolite hydroxyl group with adsorbed acetonitrile according to the four- (a) and seven-dimensional (b) model. Wavenumbers are in cm^{-1}, intensity is in 10^5 m^2/mol. The spectrum on the bottom line represents the full infrared spectrum. From bottom to top then follow the partial spectra of the hydrogen stretch, in-plane bending, out-of-plane bending, and the acetonitrile center of mass stretch mode and, for the seven-dimensional model the partial spectra of the oxygen stretch, in-plane bending, and out-of-plane bending.

caused by the symmetry of the molecule. The peak at 2773 cm^{-1} represents a combination band of the hydrogen stretch and the acetonitrile center of mass stretch mode. From the partial acetonitrile stretch spectrum it can be seen that the acetonitrile stretch interacts with all modes where the hydrogen stretch mode is involved.

Combining the information from the coefficients of basis functions in the wave functions, and the decomposition of the spectrum, we made the following attribution of peaks in the seven-dimensional spectrum. The acetonitrile stretch mode is found at 117 cm^{-1}. The small peak at 170 cm^{-1} can be attributed to the oxygen out-of-plane bending. The peaks at 685 and 750 cm^{-1} are due to hydrogen in-plane-bending and oxygen out-of-plane bending modes, respectively. The hydrogen in-plane bending mode is found at 1199 cm^{-1}, clearly enhanced in intensity compared to the spectrum without acetonitrile. At 1603 cm^{-1} there is the hydrogen out-of-plane bending mode overtone, and at 1971 cm^{-1} a small peak due to a combined excitation of both the hydrogen and the oxygen in-plane bending modes can be observed. Then from 2467 to 2860 cm^{-1} there is the Fermi resonance region. The peak at 2467 cm^{-1} is mainly due the hydrogen in-plane bending overtone. The peaks at 2690, 2745, and 2860 cm^{-1} all contain important contributions from both the hydrogen stretch and the in-plane bending modes.

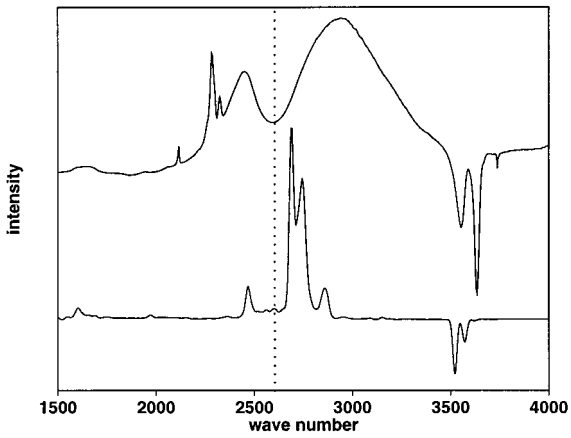

Figure 5. Experimental (top) and calculated (bottom) infrared difference spectra. Wavenumbers are in cm^{-1}. The experimental spectrum is the difference between a spectrum of a HY sample loaded with acetonitrile, and one without acetonitrile. The calculated spectrum is the difference between the calculated spectra for the six- and seven-dimensional models discussed in this paper. The dotted vertical line indicates the "Fermi dip". The sharp peaks around 2300 cm^{-1} in the experimental spectrum are due to acetonitrile CH vibrations and cannot be reproduced in our model, where acetonitrile is modeled as rigid.

The seven-dimensional spectrum displays a somewhat clearer dip in the Fermi resonance region than the four-dimensional spectrum. Also, the Fermi region is slightly shifted to higher frequency, however leaving the dip around the experimentally observed 2600 cm^{-1}. The shift is smaller than the upward shift of the hydroxyl group without acetonitrile, in comparison of three- and six-dimensional computations. This means that the overall calculated shift of the hydroxyl stretch frequency upon acetonitrile absorption increases if one takes into account the movements of the oxygen atom of the hydroxyl group.

The decomposition of the seven-dimensional spectrum is much less clear than that of the other spectra. This is partly due to the anharmonic coupling between the coordinates that we employed, which implies that it is impossible to assign infrared peaks to one single mode. Another factor is that the number of excited states that should be included in the decomposition to account for the observed absorption intensity is much greater than for the other spectra. The number of excited states actually included is, however, limited by computational resources.

Figure 5 shows a comparison between our six- and seven-dimensional models and an experimental difference spectrum. In this figure the infrared spectrum of a sample of HY is subtracted from the same sample after absorption of acetonitrile.[4] We compare it with the difference between our calculated spectra of the seven- and six-dimensional models.

There is good agreement on the position of the Fermi resonance "dip" between experiment and our calculations. Also the fact that the low-frequency band is smaller in intensity than the high-frequency band is reflected in the calculation. What is clearly lacking in the calculation is the overall width of the A,B-diad. Furthermore, the correspondence of the two peaks in the free hydroxyl stretch region is deceptive. In the experimental spectrum the lower frequency "free" hydroxyl band is due to a hydroxyl that forms a weak hydrogen bridge in HY. The low-frequency band in the calculated spectrum in this region represents the free hydroxyl stretch mode and corresponds to the higher frequency band in the experimental spectrum. The highest frequency band in the calculated spectrum corresponds to a hot band (vide supra) that is not present in the experimental

spectrum and is presumably an artifact of the cluster model and limited number of coordinates we used.

The physical picture that is used in the explanation of the A,B-spectra in several empirical models is based on a model that assumes a very strong coupling β between the acidic hydroxyl stretch mode, and the intermolecular stretch mode of the adsorbed base with respect to the hydroxyl.[6−8] We call this model I. In a discrete level model this means that combination and difference bands of the hydroxyl stretch mode with many of the overtones of the intermolecular stretch modes determine the bandwidth. The coupling β' between the hydroxyl stretch and the in-plane bending overtone in this model is relatively weak compared to β.

There is, however, an alternative explanation of the same type of spectrum possible, with $\beta \ll \beta'$ (model II). In this model the overall bandwidth is controlled by the coupling parameter β' of the hydroxyl stretch and the in-plane bending mode.

In previous discussions model I has been adopted because it agrees with the empirical law that the half-width of a shifted OH stretch band equals approximately three-fourths of the shift itself (see ref 29 and references therein). This relationship holds well for a number of experimental data, if for A,B-band systems the half-width of the shifted hydroxyl stretch bands is taken to be the overall width of the A,B-system.

However, our calculations point in the direction of a situation between the extremes presented by model I and model II. From Figure 4 we deduce values of $\beta \approx 200$ cm^{-1} and $\beta' \approx 230$ cm^{-1}. The value of β for model I would need to be approximately 800 cm^{-1}. Although the potential energy surface we employed leaves room for some improvement, we do not think a better surface would give a significantly different result. For model II a value of β approximately 300 cm^{-1} would suffice to explain the same spectrum. If the hydroxyl stretch mode in our model is shifted slightly downward, peak A in Figure 4 would broaden and reproduce the width of the experimental spectrum.

Conclusions

Using a six-coordinate vibrational model for the bridged OH group in a zeolite, we compute a value of 3522 cm^{-1} for the OH stretch frequency, which is only 2.4% below the experimental value. Vibrational models with three coordinates yield a value of 3375 cm^{-1}, which is off by 6.5%. The improvement in the six-dimensional computation is due to the coupling of the low-frequency oxygen modes with the hydrogen modes.

In the computed infrared spectrum of a zeolite-bridged OH with adsorbed acetonitrile, the dip indicating a Fermi resonance is at the same position as in the experimental spectrum. In experimental spectra the position of the dip is rather independent of the strength of the adsorbed base, so we can conclude that the cluster model describes the zeolite-bridged OH well. The computed shift of the OH band, however, is too small, indicating that the interaction between the OH group and the acetonitrile molecule is not described sufficiently by the used potential. Factors of importance are the quality description of the hydrogen bridge by the used density functional and the lack of interaction with the zeolite wall in our model.

The general shape of the computed seven-dimensional spectrum is not smooth enough. More vibrational modes will be needed to get a better approximation of the experimental spectrum. The method we used in the current work is not suited to higher dimensional models.

Our calculations indicate that it is possible to interpret A,B-type Fermi resonance spectra with a coupling of the hydroxyl stretch with the stretch mode of the adsorbed base of the order of 300 cm^{-1}, if the coupling between the hydroxyl stretch and in-plane bending overtone modes is considered to be of the order of 300 cm^{-1}, i.e., approximately the width of one of the A,B-bands appearing in the infrared spectrum.

Acknowledgment. This work has been performed under the auspices of NIOK, The Netherlands Insitute for Catalysis research, Lab Report No. TUE-98-5-07.

References and Notes

(1) Zecchina, A.; Geobaldo, F.; Spoto, G.; Bordiga, S.; Ricchiardi, G.; Buzzoni, R.; Petrini, G. *J. Phys. Chem.* **1996**, *100*, 16584.
(2) Neyman, K. M.; Strodel, P.; Ruzankin, S. Ph.; Schlensog, N.; Knözinger, H.; Rösch, N. *Catal. Lett.* **1995**, *31*, 273.
(3) Bonn, M.; Brugmans, M. J. P.; Kleyn, A. W.; van Santen, R. A. *Chem. Phys. Lett.* **1995**, *233*, 309.
(4) Pelmenschikov, A. G.; van Santen, R. A.; Jänchen, J.; Meijer, E. *J. Phys. Chem.* **1993**, *97*, 11071.
(5) Pelmenschikov, A. G.; van Wolput, J. H. M. C.; Jänchen, J.; van Santen, R. A. *J. Phys. Chem.* **1995**, *99*, 3612.
(6) Evans, J. C.; Wright, N. *Spectrochim. Acta* **1960**, *16*, 352.
(7) van Santen, R. A. *Recl. Trav. Chim. Pays-Bas* **1994**, *113*, 423.
(8) Kubelková, L.; Kotrla, J.; Florián, J. *J. Phys. Chem.* **1995**, *99*, 10285.
(9) Meijer, E. L.; van Santen, R. A.; Jansen, A. P. J. *J. Phys. Chem.* **1996**, *100*, 9282.
(10) Becke, A. D. *J. Chem. Phys.* **1993**, *98*, 5648.
(11) Becke, A. D. *Phys. Rev. A* **1988**, *38*, 3098.
(12) Lee, C.; Wang, W.; Parr, R. G. *Phys. Rev. B* **1988**, *37*, 785.
(13) Vosko, S. H.; Wilk, L.; Nusair, M. *Can. J. Phys.* **1980**, *58*, 1200.
(14) Frisch, M. J.; Trucks, G. W.; Schlegel, H. B.; Gill, P. M. W.; Johnson, B. G.; Wong, M. W.; Foresman, J. B.; Robb, M. A.; Head-Gordon, M.; Replogle, E. S.; Gomperts, R.; Andres, J. L.; Raghavachari, K.; Binkley, J. S.; Gonzalez, C.; Martin, R. L.; Fox, D. J.; Defrees, D. J.; Baker, J.; Stewart, J. J. P.; Pople, J. A. *Gaussian 92/DFT, Revision F.2;* Gaussian, Inc.: Pittsburgh, PA, 1993.
(15) Hehre, W. J.; Stewart, R. F.; Pople, J. A. *J. Chem. Phys.* **1969**, *51*, 2657.
(16) Krishnan, R.; Binkley, J. S.; Seeger, R.; Pople, J. A. *J. Chem. Phys.* **1973**, *72*, 650.
(17) Clark, T.; Chandrasekhar, J.; Spitznagel, G. W.; Schleyer, P. v. R. *J. Comput. Chem.* **1982**, *4*, 294.
(18) Defrees, D. J.; McLean, A. D *J. Comput. Chem.* **1986**, *7*, 321.
(19) Gordon, M. S.; Binkley, J. S.; Pople, J. A.; Pietro, W. J.; Hehre, W. J. *J. Am. Chem. Soc.* **1982**, *104*, 2797.
(20) Hehre, W. J.; Ditchfield, R.; Pople, J. A. *J. Chem. Phys.* **1971**, *56*, 2257.
(21) Francl, M. M.; Pietro, W. J.; Hehre, W. J.; Binkley, J. S.; Gordon, M. S.; Defrees, D. J.; Pople, J. A. *J. Chem. Phys.* **1986**, *77*, 3654.
(22) Hariharan, P. C.; Pople, J. A. *Theor. Chim. Acta* **1973**, *28*, 213.
(23) Press: W. H.; Flannery, B. P.; Teukolsky, S. A.; Vetterling, W. T. *Numerical Recipes in C, The Art of Scientific Computing;* Cambridge University Press: Cambridge, 1988; Chapter 2.9.
(24) Wilson, E. B., Jr.; Decius, J. C.; Cross, P. C. *Molecular Vibrations;* Mc-Graw-Hill: New York, Toronto, London, 1955.
(25) Wilson, Jr., E. B.; Decius, J. C.; Cross, P. C. *Quantum Mechanics;* John Wiley & Sons: New York, 1955; Chapter XII.
(26) Pauling, L.; Wilson, E. B. *Introduction to Quantum Mechanics;* McGraw-Hill: 1935; Chapter XI.
(27) Lewis, J. G. *Algorithms for sparse matrix eigenvalue problems;* Stanford University, Department Computer Science: Stanford, CA, 1977; Chapter 3.4.
(28) Parlett, B. N *The Symmetric Eigenvalue Problem;* Prentice Hall: Englewood Cliffs, NJ, 1980.
(29) Pimentel, G. C.; McClellan, A. L. *The Hydrogen Bond;* W. H. Freeman and Company: San Francisco and London, 1960; Chapter 3.